Dakshinamurthy, M. y Ma, A. (2018). Crack propagation in TRIP assisted steels modeled by crystal plasticity and cohesive zone method. *Theoretical and Applied Fracture Mechanics*, 96, pp. 545-555.

DOI: https://doi.org/10.1016/j.tafmec.2018.06.005

Crack propagation in TRIP assisted steels modeled by crystal plasticity and cohesive zone method

Manjunath Dakshinamurthy[a], Anxin Ma[b,*]

[a] *Nonlinear Solid Mechanics group, Department of Continuum Mechanics and Structural Analysis, Universidad Carlos III Madrid, Spain*
[b] *IMDEA Materiales, C/Eric Kandel, 2, Tecnogetafe, 28906 Getafe, Madrid, Spain*

A B S T R A C T

The influence of transformation induced plasticity (TRIP) on materials mechanical behaviours, as well as failure phenomena including crack propagation and phase boundary debonding in multiphase steels (e.g. dual phase steels, TRIP steels) are studied by using an advanced crystal plasticity finite element method. We have coupled the crystal plasticity model Ma and Hartmaier (2015), which explicitly considers elastic-plastic deformation of ferrite and austenite, austenite-martensite phase, with a cohesive zone model designed for crack propagation, to study the deformations of several representative microstructural volume elements (RVE). Results shows that, the transformation induced plasticity enhances materials strength and ductility, hinders crack propagation and in-fluences interface debonding. Furthermore, the martensitic transformation kinetics in TRIP steels was found depending on the crystallographic orientation and the stress state of a retained austenite grain. The current simulation results helps to investigate and design multiphase steels with improved mechanical properties.

Keywords:
Crystal plasticity
Metastable austenite
Transformation induced plasticity (TRIP)
Cohesive zone method
Martensite versus ferrite-martensite cracking

1. Introduction

Applications of the steel require them to be both strong and ductile. Multiphase steels like dual phase steels and TRIP (Transformation induced plasticity) steels are the front runners of advanced high strength steels for automotive applications. The name dual phase steels was coined to describe ferrite-martensite microstructure by Rashid [35], but dual phase steels usually contains more than two phases unlike implied by their name. With high ultimate tensile strength, combined with low initial yielding stress [12,11], dual phase steels form an ideal alloy system for automotive applications, where a good combination of cold formability and strength is required as reported by Tasan et al. [38]. These steels presents complex multiphase microstructure, consisting of ferritic matrix and a dispersion of multiphase grains of bainite, martensite and meta-stable retained austenite [3,32]. The increased strength and ductility in multiphase steels, such as, dual phase and TRIP steels can be credited to the coexistence of softer and harder phases. TRIP assisted multiphase steels, presents extra-strain hardening contribution, brought about by the continuous transformation under loading of one of the phase (austenite), into a harder phase martensite Lebedev and Kosarchuk [22]. The complex microstructure and heterogeneity, makes it harder to understand the multiphase steels to complete extent and to unlock the full potential of multiphase steels.

Another aspect to the studying of multiphase steels is, understanding the complex damage and failure behaviour of these steels. It is know from previous studies that, DP steels are prone to nucleating micro-cracks, because of the presence of martensite in the microstructure. From the fundamental viewpoint, outstanding issues like relationship between mechanically induced martensitic transformation, fracture toughness, stress-state dependency and the damage mechanism taking place with in the evolving multiphase microstructure [34,25,26,14,19,10,28] have not yet been clarified. Owing to these complexities, numerous investigations on the effect of retained austenite on fracture toughness and damage mechanism have been carried out. The next challenge, in studying damage mechanism in DP steels is, the relative activity of martensite cracking versus ferrite-martensite interface debonding. Variety of damage mechanism have been reported in literature, for example [18,17], showed that the fracture of martensite particle dominates over interface debonding of ferrite and martensite particle. Studies of [9,4,29] have shown that, different damage mechanisms of particular dual phase steels are related also to their chemical compositions, heat treatment history, and differences in their final microstructure. Avramovic-Cingara et al. [2] suggested that the major void nucleation mechanism is decohesion at the ferrite/martensite interface, and these voids grow along ferrite grain boundaries. Maire et al. [24] reported that, they observed both martensitic fracture and ferrite/martensite decohesion during their in situ tensile test. The influence of martensite volume fraction, ferrite grain size,

* Corresponding author.
E-mail addresses: mdakshin@ing.uc3m.es (M. Dakshinamurthy), anxin.ma@imdea.org (A. Ma).

martensite morphology on martensite cracking and ferrite martensite interface debonding is presented in detail by Tasan et al. [38]. The damage processes are dynamic, and thus martensite cracking and ferrite-martensite interface debonding incident resemble each other. The complexity of differentiating between them in experiments, increases the need for simulations that can shed some light on this process.

On the micro scale, two failure modes have been found to be operational in parallel: cleavage and dimple fracture [32]. Numerous, experimental and numerical studies have been performed over the years, to explain the damage mechanism in dual phase steels. Studies of [15,16,20,5] have reported, different types of damage mechanisms from their experimental work with the help of SEM and light optical microscopy. It has also been reported, on the influence of stress state on the rate of martensitic transformation and the effect of martensitic transformation on damage mechanism [34,19,14]. Large number of numerical work has also been carried out to support the experimental findings. Various approach has been applied using RVE's (representative volume element), within the framework of continuum mechanics, to consider the influence of multiphase microstructure [42,43,34,16,6]. The numerical simulation of damage and crack propagation with the finite element method is performed using GTN approach and phenomenological model (cohesive zone method).

In the present work, a crystal plasticity based model has been employed for modeling mechanical response of materials. The constitutive model for TRIP assisted steels, based on the thermodynamic principle of Ma and Hartmaier [23] is adopted. This model, uses inverse NW orientation relationship, sets explicit connections between the strain induced martensite nucleation and plastic deformation of austenite, and considers stress-assisted growth and strain induced nucleation at the same time. The cleavage failure mechanism is described using cohesive zone model, the phenomenological model describes fracture as material separation due to an achieved critical condition. Main focus of the current work is to combine the above mentioned methods to study the influence of phase transformation on global mechanical behaviour of material, to study the factors affecting crack propagation speed and direction, and to study the effect of austenite to martensite transformation on the cleavage failure mechanism.

2. Description of the constitutive model

2.1. Constitutive model for ferrite

2.1.1. Kinematics

Following the multiplicative decomposition approach, the deformation gradient tensor $\mathbf{F}$ can be separated into an elastic deformation part $\mathbf{F}^{\mathrm{e}}$ and a plastic deformation part $\mathbf{F}^{\mathrm{p}}$, as follows

$$\mathbf{F} = \mathbf{F}^{\mathrm{e}}\mathbf{F}^{\mathrm{p}}. \tag{1}$$

2.1.2. Elasticity

With the help of an elastic stiffness tensor of ferrite, $\mathbb{C}^{\mathrm{fer}}$, we calculate the second Piola-Kirchhoff stress in the intermediate configuration

$$\widetilde{\mathbf{S}} = \mathbb{C}^{\mathrm{fer}}\left[\frac{1}{2}(\mathbf{F}^{\mathrm{e}\mathrm{T}}\mathbf{F}^{\mathrm{e}} - \mathbf{I})\right]. \tag{2}$$

2.1.3. Plasticity

Provided that the initial plastic deformation gradient $\mathbf{F}^{\mathrm{p}0}$ and a small time increment Δt are given, inside the large deformation framework the current plastic deformation gradient amounts to

$$\mathbf{F}^{\mathrm{p}} = \left(\mathbf{I} + \sum_{\alpha=1}^{N^S} \dot{\gamma}_\alpha \Delta t \widetilde{\mathbf{M}}_\alpha\right)\mathbf{F}^{\mathrm{p}0} \tag{3}$$

where $\dot{\gamma}_\alpha$ and $\widetilde{\mathbf{M}}_\alpha$ are the shear rate and the slip system Schmid tensor of slip system α, respectively.

Table 1
Slip systems $\widetilde{\mathbf{M}}_\alpha$ of the BCC crystal structure.

α	$\widetilde{\mathbf{d}}_\alpha \otimes \widetilde{\mathbf{n}}_\alpha$	α	$\widetilde{\mathbf{d}}_\alpha \otimes \widetilde{\mathbf{n}}_\alpha$
1	$[1\,1\,1] \otimes (0\,1\,\bar{1})/\sqrt{6}$	7	$[1\,\bar{1}\,1] \otimes (0\,1\,1)/\sqrt{6}$
2	$[1\,1\,1] \otimes (1\,0\,\bar{1})/\sqrt{6}$	8	$[1\,\bar{1}\,1] \otimes (1\,0\,\bar{1})/\sqrt{6}$
3	$[1\,1\,1] \otimes (1\,\bar{1}\,0)/\sqrt{6}$	9	$[1\,\bar{1}\,1] \otimes (1\,1\,0)/\sqrt{6}$
4	$[\bar{1}\,1\,1] \otimes (\bar{1}\,1\,1)/\sqrt{6}$	10	$[1\,1\,\bar{1}] \otimes (0\,1\,1)/\sqrt{6}$
5	$[\bar{1}\,1\,1] \otimes (1\,0\,1)/\sqrt{6}$	11	$[1\,1\,\bar{1}] \otimes (1\,0\,1)/\sqrt{6}$
6	$[\bar{1}\,1\,1] \otimes (1\,1\,0)/\sqrt{6}$	12	$[1\,1\,\bar{1}] \otimes (1\,\bar{1}\,0)/\sqrt{6}$

Because, the body centered cubic (BCC) crystal structure has no truly close packed planes, it is very difficult to determine the active glide systems.It has been observed experimentally that dislocations glide on the $\{1\,1\,0\}$ planes. Hence, with respect to the $N^{\mathrm{S}} = 12$ slip systems listed in Table 1, we adopt the phenomenological visco-plastic type flow law

$$\dot{\gamma}_\alpha = \dot{\gamma}_0 \left|\frac{\tau_\alpha}{\hat{\tau}_\alpha}\right|^{p_1} \mathrm{sign}(\tau_\alpha). \tag{4}$$

with the resolved shear stress

$$\tau_\alpha = \widetilde{\mathbf{S}} \cdot \widetilde{\mathbf{M}}_\alpha \tag{5}$$

where the parameter $\dot{\gamma}_0$ is the reference shear rate, p_1 the reciprocal value of the strain rate sensitivity.

2.1.4. Hardening

The critical resolved shear stress $\hat{\tau}_\alpha$, obeys the following evolution rule

$$\dot{\hat{\tau}}_\alpha = \sum_{\beta=1}^{N^S} h_0 \chi_{\alpha\beta}\left(1 - \frac{\hat{\tau}_\beta}{\hat{\tau}_{\mathrm{s}}}\right)^{p_2} |\dot{\gamma}_\beta| \tag{6}$$

where h_0 is the initial hardening rate, $\hat{\tau}_{\mathrm{s}}$ the saturation resistance, p_2 the power and $\chi_{\alpha\beta}$ the cross hardening coefficient matrix.

2.2. Constitutive model for austenite

The crystal plasticity model used for modeling metastable austenitic and martensitic transformation is an integrated form of the models proposed by Ma and Hartmaier [23]. A short description of the constitutive formulations for martensitic phase transformation is presented in this section. For retained austenite grain, the total deformation gradient can be decomposed into elastic $\mathbf{F}^e$, plastic $\mathbf{F}^t$ and transformation $\mathbf{F}^p$ part, through introducing two intermediate configuration, $\widetilde{\mathbf{x}}'$ and $\widetilde{\mathbf{x}}$, respectively multiplicatively as shown in Eq. (7).

$$\mathbf{F} = \frac{\partial \mathbf{x}}{\partial \widetilde{\mathbf{x}}'}\frac{\partial \widetilde{\mathbf{x}}'}{\partial \widetilde{\mathbf{x}}}\frac{\partial \widetilde{\mathbf{x}}}{\partial \mathbf{X}} = \mathbf{F}^e\mathbf{F}^p\mathbf{F}^t \tag{7}$$

The plastic deformation is caused by dislocation slip on crystallographic slip systems. The martensite transformation mechanism includes martensite nucleation and the growth of the martensite nuclei. As the pre-existing nuclei are crucial to consider the martensitic phase transformation taking place before yielding, the total evolution of martensite can be additively decomposed into pre-existing nuclei of martensite $\boldsymbol{\eta}^0$, strain induced nucleation $\boldsymbol{\eta}^{\mathrm{strain}}$, stress assisted growth $\boldsymbol{\eta}^{\mathrm{stress}}$ as follow

$$\boldsymbol{\eta} = \boldsymbol{\eta}^0 + \boldsymbol{\eta}^{\mathrm{strain}} + \boldsymbol{\eta}^{\mathrm{stress}}. \tag{8}$$

The transformation caused deformation amounts to

$$\dot{\mathbf{F}}^t = \sum_{I=1}^{N^T} \dot{\eta}_I^{\mathrm{stress}} \widetilde{\mathbf{N}}_I \tag{9}$$

where N^T is the number of transformation systems. $\widetilde{\mathbf{N}}_I$ is the eigen deformation tensor of the inverse NW relation.

2.2.1. Elasticity

Elastic law in the current configuration is given by:

$$\boldsymbol{\sigma} = \frac{1}{\det(\mathbf{F}^{\mathrm{e}})}\mathbf{F}^{e}\left[\mathbb{C}\frac{1}{2}(\mathbf{F}^{eT}\mathbf{F}^{e}-\mathbf{I})\right]\mathbf{F}^{eT} \tag{10}$$

The stresses in the configuration $\widetilde{\mathbf{x}}$ for dislocation slip and at the same time in the configuration $\widetilde{\mathbf{x}}'$ for phase transformation are

$$\widetilde{\mathbf{S}} = \det(\mathbf{F}^{e})\mathbf{F}^{e-1}\boldsymbol{\sigma}\mathbf{F}^{e-\mathrm{T}} \tag{11}$$

$$\widetilde{\mathbf{S}}' = \det(\mathbf{F})\mathbf{F}^{t-1}\mathbf{F}^{e-1}\boldsymbol{\sigma}\mathbf{F}^{e-\mathrm{T}}\mathbf{F}^{t-1} \tag{12}$$

2.2.2. Plasticity and hardening

The driving force for plastic shear in slip system α

$$\zeta_{\alpha}^{\mathrm{p}} = \tau_{\alpha}-(\hat{\tau}_{\alpha} + \hat{\tau}_{\alpha}^{\mathrm{t}})\mathrm{sign}(\dot{\gamma}_{\alpha}) = \tau_{\alpha}-(\hat{\tau}_{\alpha}^{\mathrm{p}} + \hat{\tau}_{\alpha}^{\mathrm{t}})\mathrm{sign}(\tau_{\alpha}) \tag{13}$$

with

$$\tau_{\alpha} = \frac{\det(\mathbf{F})}{2}\boldsymbol{\sigma}\cdot(\mathbf{F}^{\mathrm{e}}\mathbf{F}^{\mathrm{t}}\widetilde{\mathbf{M}}_{\alpha}\mathbf{F}^{\mathrm{t}-1}\mathbf{F}^{\mathrm{e}-1} + \mathbf{F}^{\mathrm{e}\text{-}\mathrm{T}}\mathbf{F}^{\mathrm{t}\text{-}\mathrm{T}}\widetilde{\mathbf{M}}_{\alpha}^{\mathrm{T}}\mathbf{F}^{\mathrm{t}\mathrm{T}}\mathbf{F}^{\mathrm{e}\mathrm{T}}) \tag{14}$$

where the shear rate, $\dot{\gamma}_{\alpha}$, is assumed to take the same direction as the resolved shear stress, τ_{α}.

A phenomenological power law is assumed for the shear rate $\dot{\gamma}_{\alpha}$,

$$\dot{\gamma}_{\alpha} = \dot{\gamma}_{0}\left|\frac{\zeta_{\alpha}^{\mathrm{p}}}{\hat{\tau}_{0}}\right|^{p_1}\mathrm{sign}(\tau_{\alpha}) \tag{15}$$

Another phenomenological type strain and martensite lamellar hardening law is assumed for the present work.

$$\dot{\hat{\tau}}_{\alpha}^{\mathrm{p}} = \sum_{\beta=1}^{N_{\mathrm{S}}} h_{0}\chi_{\alpha\beta}\left(1-\frac{\hat{\tau}_{\beta}^{\mathrm{p}}}{\hat{\tau}_{\mathrm{s}}}\right)^{p_2}|\dot{\gamma}_{\beta}| \tag{16}$$

2.2.3. Strain induced martensite nucleation

By solving the energy minimization control equations, a driving force for strain induced martensite nucleation

$$\zeta_{I}^{\mathrm{strain}} = -[12\Delta\mathrm{G}(\eta_{I}^{2}-\eta_{I}^{3})] \tag{17}$$

and a fault band intersection probability $\dot{P}_I$, which is function of shears on slip systems of austenite, may help us to formulate the martensite nucleation rate

$$\dot{\eta}_{I}^{\mathrm{strain}} = C^{\mathrm{nuc}}\left(1-\sum_{J=1}^{N^{\mathrm{T}}}\eta_{\mathrm{J}}\right)\dot{P}_{I}\zeta_{I}^{\mathrm{strain}}\dot{\gamma}_{\alpha} \tag{18}$$

where C^{nuc} is a fitting parameter, η_I is the volume fraction of transformed martensite at transformation system I. The free energy difference between austenite and martensite, ΔG, is a function of temperature and alloy concentration.

2.2.4. Stress assisted martensite growth

The driving force for stress assisted martensitic transformation is

$$\zeta_{I}^{\mathrm{stress}} = \det(\mathbf{F})\boldsymbol{\sigma}\cdot\frac{1}{2}(\mathbf{F}^{\mathbf{e}}\widetilde{\mathbf{N}}_{I}\mathbf{F}^{\mathbf{e}^{-1}} + \mathbf{F}^{\mathbf{e}^{-\mathrm{T}}}\widetilde{\mathbf{N}}_{I}^{T}\mathbf{F}^{\mathbf{e}^{\mathrm{T}}}) + [12\Delta\mathrm{G}(\eta_{I}^{2}-\eta_{I}^{3})]. \tag{19}$$

Considering the sigmoidal profile for the kinetics of martensitic transformation,the rate of stress assisted growth can be defined as

$$\dot{\eta}_{I}^{\mathrm{stress}} = C^{\mathrm{gro}}(\eta_{I}^{0} + \eta_{I}^{\mathrm{strain}})\left(1-\sum_{\beta=1}^{N^{\mathrm{T}}}\eta_{\beta}\right)\zeta_{I}^{\mathrm{stress}}, \tag{20}$$

where C^{gro} is the temperature dependent fitting parameter and η_I^0 is the pre-existing nuclei available for growth.

Table 2
Model parameters for plasticity.

Parameter	Notation	Ferrite	Austenite
Reference shear rate	$\dot{\gamma}_0$ (s^{-1})	0.001	0.001
Reciprocal of strain rate sensitivity	p_1	45.5	200
Initial critical resolved shear stress	$\hat{\tau}_0$ (MPa)	40	150
Initial strain hardening rate	h_0 (MPa)	500	345
Saturated critical resolved shear stress	$\hat{\tau}_s$ (MPa)	117	480
Strain hardening power	p_2	5	2.25
Co-planar hardening coefficient	$\chi_{\alpha\beta}$	1	1
Other hardening coefficient	$\chi_{\alpha\beta}$	1.4	1.4

Table 3
Model parameters for retained austenite with TRIP.

Parameters	Notation	Value
Coefficient of martensite nucleation	C^{nuc}	0.0028
Coefficient of martensite growth	C^{gro}	0.007
Bulk energy difference	ΔG (MPa)	−150

Table 4
Model parameter for elasticity.

Parameter	Ferrite	Austenite	Martensite
c_{11} (GPa)	231.4	242.0	242.0
c_{12} (GPa)	134.7	146.5	146.5
c_{44} (GPa)	116.4	112.0	112.0

Once the martensitic transformation is complete, the newly formed martensite is treated as an elastic material with the same elastic parameters as austenite. The model parameters for elasticity, plasticity and phase transformation are given in Tables 4, 2, 3.

2.3. Cohesive zone model

Cleavage fracturing, in the RVE's are described using the cohesive model on a local scale. Cohesive surface, representing damage is created between continuum elements. The cohesive surface open when damage occurs and lose their stiffness at failure, causing the continuum elements to become disconnected. For this reason, the crack can only propagate along the element boundaries and the possible crack path must be defined during the mesh generation procedure. In this work, it is assumed that, the separation process is dominated by normal fracturing, and the cohesive surface are therefore created in the overall middle plane of the RVE model shown in Fig. 2. The damage process is controlled by a traction-separation law (TSL), simulating the deformation and finally the decohesion of a material in the immediate vicinity of the crack tip. The constitutive response of the cohesive zone method is defined directly in terms of traction versus separation behaviour. The traction – separation model assumes, initially linear elastic behaviour, followed by initiation and evolution of damage. In the present work, a bi-linear traction separation behaviour, as shown in Fig. 1 is used. The cohesive zone model has been implemented in Abaqus [1] in terms of cohesive elements and also cohesive surfaces. Each failure mechanism consists of two ingredients: a damage initiation criterion and a damage evolution law upon reaching a completely damaged state. The process of degradation begins when the stresses satisfy certain damage initia-tion criteria that we specify. Maximum stress criterion is been used in the present work. The damage is assumed to initiate when the max-imum nominal stress ratio reaches a value of one. This criterion can be represented as:

$$\max\left\{\frac{t_n}{t_n^o}, \frac{t_s}{t_s^o}, \frac{t_t}{t_t^o}\right\} = 1 \tag{21}$$

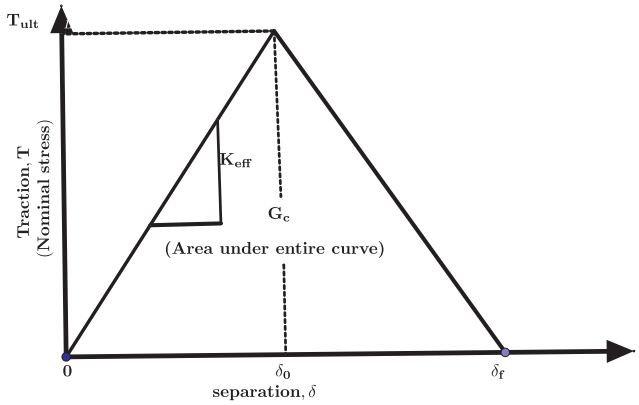

Fig. 1. Bi-Linear traction – separation model.

t_n^0, t_s^0 and t_t^0 represent the peak values of the nominal stress when the deformation is either purely normal to the interface or purely in the first or the second shear direction, respectively.

2.4. Representative volume element

2.4.1. Geometry

The RVE's used for simulation consists of 10 mm× 10 mm × 0.1 mm cube, containing circular Inclusion and ferrite matrix, volume of the inclusion is around 10%. To investigate the influence of TRIP on cleavage failure mechanism and the effect of stress state on transformation induced plasticity, a matrix-inclusion type plane strain quasi 2D (one element in *Z* direction) RVE is used. The complete simulation zone for matrix-inclusion is discretized into 10000 C3D8R elements.

For studying the cleavage mechanism, a cohesive surface model with pre-defined crack path is used. Separate cohesive surfaces are used to model ferrite-ferrite and austenite-ferrite, and martensite-martensite interfaces, as shown in Fig. 2 (Red lines highlighted in the figure shows the cohesive surface). The CZ parameter listed in Table 5 are taken from literature Uthaisangsuk et al. [42]. A small notch is created on the left side of the RVE on the crack path, so that crack always initiates from here and move towards inclusion.

The orientation of retained austenite inclusion, ferrite matrix, martensite inclusion are given in terms of Bunge Euler angles, as shown in Table 6. The Euler angles are defined with respect to the global basis.

Three different representative microstructural volume elements (RVE), representing three different microstructures are created, the main difference between each RVE is, the material in the inclusion. In the modeling part, we have given description of model used for retained austenite with transformation [TRIP RVE], same model is used for martensite [FM-DP-RVE] and retained austenite without transformation [FA-DP-RVE], by changing the amount of martensitic transformation. For retained austenite without transformation [FA-DP-RVE], martensitic transformation is set to zero, at all the time of calculation, this can be done by neglecting the $\mathbf{F}^t$ part of deformation gradient. Similarly, for FM-DP-RVE with martensite inclusion, initial martensitic volume fraction is set to 1, i.e., 100% martensite and is maintained throughout the simulation. For TRIP-RVE, initial martensitic volume fraction is set to 0.02 and allowed to grow during the simulation.

- FM-DP: ferrite matrix with martensite inclusion.
- FA-DP: ferrite matrix with austenite.
- TRIP: ferrite matrix with meta-stable austenite inclusion with phase transformation (TRIP).

2.4.2. Boundary conditions

Initially stress free RVE's are subjected uniaxial tensile loading, as shown in Fig. 2. Uniaxial tensile load, in terms of normal displacement is applied along Y direction. The normal (X) displacements on right and left face of the RVE are set to zero, all the degrees of freedom along Z directions are set free (unconstrained).

A user material subroutine UMAT is developed in the framework of

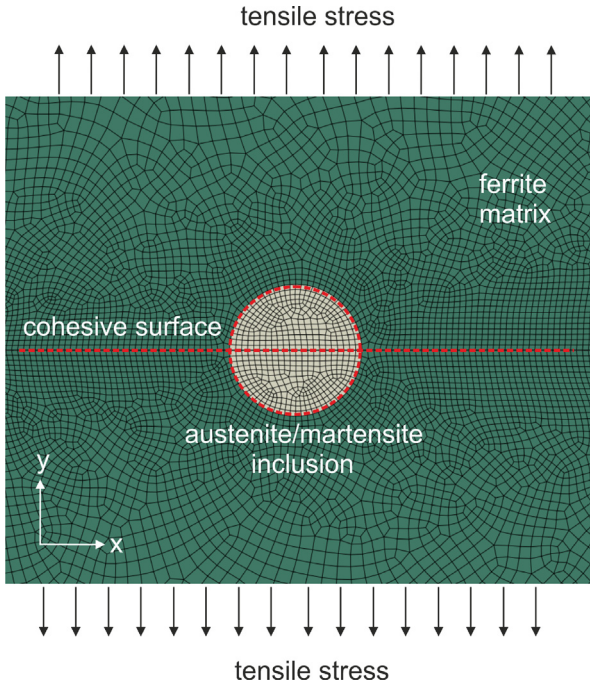

Fig. 2. Matrix-inclusion type finite element model with boundary conditions. The circular inclusion, in the middle of the matrix (White coloured) is austenite/martensite. The green part of matrix is Ferrite. The predefined cohesive surfaces are highlighted. (For interpretation of the references to color in this figure legend, the reader is referred to the web version of this article.)

Table 5
Parameters for cohesive zone model.

Parameter	Notation	Value
Initial stiffness of ferrite	K_{eff} (MPa/mm)	210,000
Initial stiffness of martensite	K_{eff} (MPa/mm)	210,000
Initial stiffness of austenite	K_{eff} (MPa/mm)	210,000
maximal traction of ferrite	T_{ult} (MPa)	1500
maximal traction of martensite	T_{ult} (MPa)	1200
maximal traction of austenite	T_{ult} (MPa)	1200
cohesive energy of ferrite	G_c (J/mm^2)	495
cohesive energy of austenite	G_c (J/mm^2)	100
cohesive energy of martensite	G_c (J/mm^2)	100

Table 6
Orientation of austenite/martensite inclusion and ferrite matrix for different RVE's in terms of euler angles. The euler angles are defined with respect to global basis (x,y,z).

RVE	Matrix orientation (Bunge euler angles)	Inclusion orientation (Bunge euler angles)	miller indices for inclusion (parallel to Y direction)
FA-DP-RVE	(0, 0, 0)	(0, 0, 0)	[1 0 0]
FM-DP-RVE	(0, 0, 0)	(0, 0, 0)	[1 0 0]
TRIP-RVE (1 0 0)	(0, 0, 0)	(0, 0, 0)	[1 0 0]
TRIP-RVE (1 1 0)	(0, 0, 0)	(0, 45, 0)	[1 1 0]
TRIP-RVE (1 1 1)	(0, 0, 0)	(45, 35.23, 0)	[1 1 1]
TRIP-RVE (1 2 3)	(0, 0, 0)	(15.5, 56.3, 0)	[1 2 3]

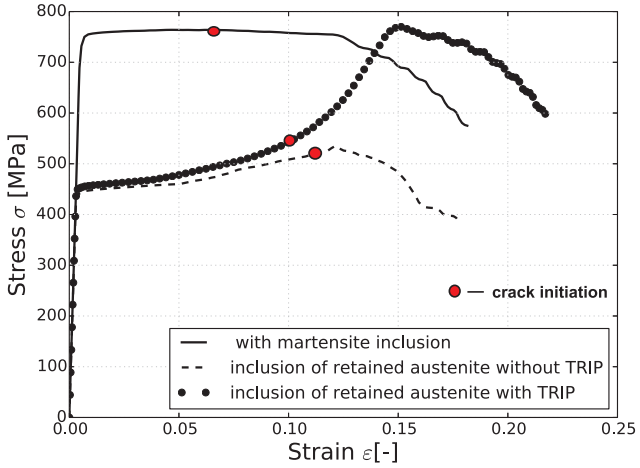

Fig. 3. Uniaxial tensile, global nominal stress-strain curve for all three RVE's. The orientation for both ferrite matrix and retained austenite/martensite inclusion is (0, 0, 0).

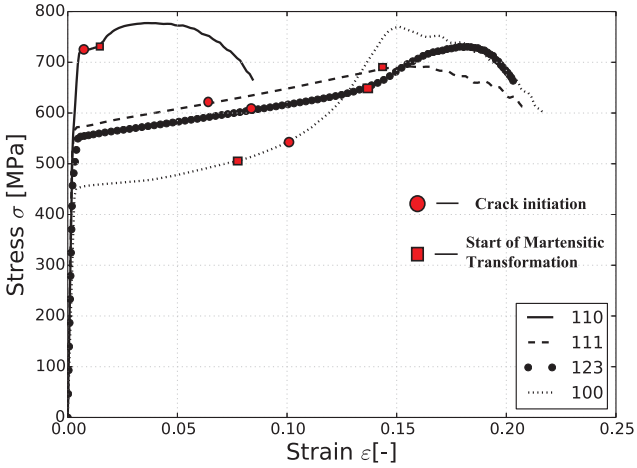

Fig. 4. Nominal stress-strain curves for TRIP-RVE with different retained austenite inclusion orientations, orientation of ferrite matrix is kept constant.

commercial ABAQUS software, which allows us to update the stress and state dependent variables (SDVs) at the end of each time increment. The constitutive formulation of UMAT should be such that it must return stress σ and stiffness $\frac{d\sigma}{d\epsilon}$, for the global non-linear solution.

3. Results and discussion

3.1. Strength and ductility

FE calculations of the uniaxial tensile tests are performed for three different RVE's (FM-DP, FA-DP, TRIP). From these calculations, the global stress-strain curves, local stress, strain and damage are determined. The determined flow behaviour in terms of nominal stress-strain curves is shown in Fig. 3 for different RVE's. FM-DP RVE achieves high stress values at initial stages of deformation itself, when compared to other two RVEs. The higher stress values in FM-DP RVE's is due to the presence of the martensite in RVE. TRIP RVE's exhibits low stress values initially i.e., before the transformation of austenite to martensite, but once the transformation starts, the stress value starts increasing gradually. For FA-DP-RVE, the stress values is low and continues to be almost same until the softening begins. The stress strain curves FM-DP, FA-DP RVEs forms an upper bound and lower bound for the stress strain curve of TRIP-RVE respectively. Stress and strain levels in TRIP-RVE is same as FA-DP-RVE at the initial stages of deformation, whereas at the final stages of deformation, TRIP-RVE it is identical as FM-DP-RVE. In TRIP RVE, the transformation of retained austenite to martensite brings remarkable hardening at high strain levels. Transformation induced plasticity (TRIP) effect improves both the strength and ductility, this fits well with experimental results [12,19,41,27,31,21,30,36].

At high strain levels, softening behaviour becomes more evident in all three RVEs. Softening behaviour starts dominating in FM-DP-RVE at very low strain level, as the stress starts dropping gradually in FM-DP-RVE. Martensite inclusion in FM-DP-RVE takes more load from the onset of the deformation and hence the stress levels are very high inside the martensite inclusion, this high stress state is sufficient for the da-mage initiation inside the martensite inclusion. In TRIP RVE, since the stress value is less from the initial stages of deformation, it is only after the transformation of austenite to martensite, stress starts increasing and T_{ult} is reached, hence softening starts later than FM-DP-RVE. For FA-DP-RVE, the softening behaviour starts later than both FM-DP-RVE and TRIP RVE, this could be attributed to the ductile behaviour of the austenite inclusion and its greater compatibility with ferrite matrix. The inclusion with higher local stress state failed earlier [i.e., T_{ult} is reached at low strains] when compared to the inclusions with less stress levels.

As shown in Fig. 3, ultimate stress T_{ult} required for damage initiation is reached earlier in FM-DP RVE, followed by TRIP RVE and later in FA-DP-RVE.

3.1.1. Effect of retained austenite inclusion orientation on effective strength and Ductility

In this section, effect of retained austenite inclusion orientation on martensitic transformation is presented, the set-up for the simulation is same as mentioned in the previous section. Uniaxial tensile test is performed on TRIP RVE, the major change being the orientation of the retained austenite inclusion. The orientation of the ferrite matrix remains same as before i.e., [1 0 0] for all the simulation, but the orientation of retained austenite inclusion is varied. In the present study, we consider four different orientations [1 0 0], [1 1 1], [1 1 0], [1 2 3] (orientations in terms of euler angles are mentioned in Table 6).

It is well known that crystal orientation affects mechanical behaviour of materials Gupta et al. [7], as shown in Fig. 4, our simulation results reflects the influence of orientation on mechanical response. It can be noted that the RVE with RA (retained austenite) inclusion orientation [1 1 0] reaches very high stress levels at the early stages of deformation, also there is not much of hardening before the softening behaviour dominates. Further, the effective strength of RVE's with [1 1 1], [1 2 3] oriented RA inclusion is higher than [1 0 0], this strong behaviour is because of the orientations of RA inclusion. The low effective strength of [1 0 0] is due to the capability of austenite grain to accommodate the externally imposed deformation without significant increase in stress. The [1 0 0] oriented austenite grain subjected to homogeneous uniaxial loading conditions, exhibits a low and constant stress values during the initial stages of martensitic transformation. But, once the transformation approaches completion, the stress value starts increasing. The increase in stress can be attributed to the presence of martensite in the grain, similar kind of behaviour has been reported in [40,39].

3.1.2. Martensitic transformation and orientation dependence

Fig. 5(a) shows the average amount of martensitic transformation in differently oriented RA inclusions. [1 0 0] orientation favours the martensitic transformation more, followed by [1 2 3], [1 1 1], [1 1 0] respec-tively. It is also interesting to see the rate at which martensite trans-formation happens in [1 0 0] and [1 2 3]. In [1 0 0] RVE, the rate of transformation is very high, but for [1 2 3] orientation, the martensitic transformation rate is considerable lower. Martensitic transformation starts earlier in [1 0 0] orientation, than in [1 2 3] orientation, this is because, for [1 2 3] orientation, the effective stress required for mar-tensitic transformation is high.

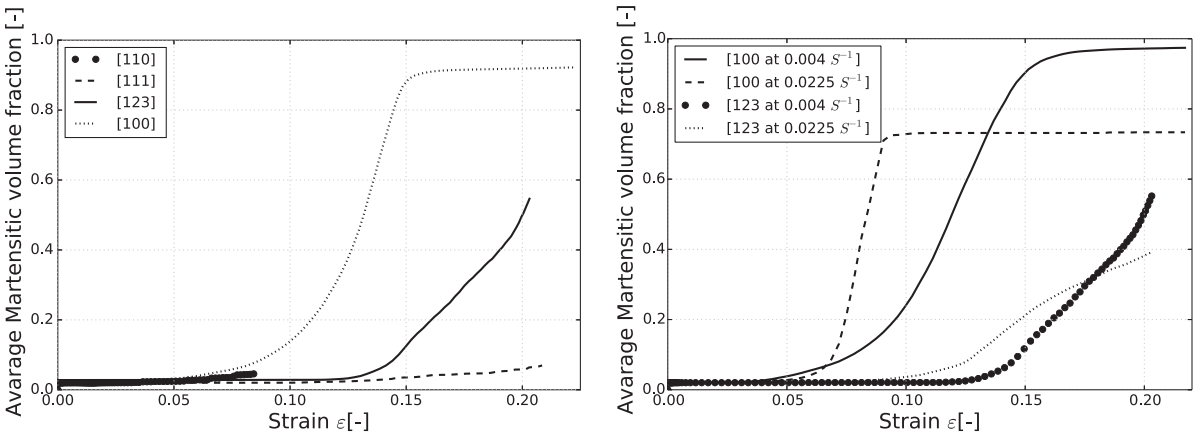

(a) Effect of orientation on martensite transformation (loading rate 0.004 s^{-1})

(b) Effect of loading rate on martensite transformation

Fig. 5. Average Martensitic volume fraction inside the TRIP-RVE inclusion, is plotted with strain. In (a) orientation of retained austenite inclusion is varied, but ferrite matrix orientation is kept constant. In (b) loading rate, but the matrix and inclusion orientations are kept constant.

The martensitic transformation inside the [1 0 0] oriented RA in-clusion is more uniformly distributed. But, for [1 2 3] orientation, mar-tensitic transformation inside the inclusion is more accumulated around the crack, this can be attributed to high stress state in front of crack, which acts as a driving force for transformation. For [1 2 3] orientation, martensitic transformation increases once the crack reaches the inclu-sion, i.e., there is huge amount of martensitic transformation in front of crack and the martensite transformation is more accumulated around the crack path, as we can see from Fig. 7. This trend continues for both [1 1 1], [1 1 0] orientations, even though the amount of martensitic transformation is lesser compared to [1 2 3]. From this, we can say that the high stress state in front of the crack, promotes the martensitic transformation.

To study the effect of loading rate on martensitic transformation, calculations are performed at two different loading rates (0.0225 s^{-1} and 0.004 s^{-1}). As we can see from Fig. 5(b), martensitic transformation starts early at high loading rate and the rate of transformation is also high, this is because of high stress state, at high loading rate. Important thing to be observed here is the amount of martensitic transformation, at high loading rate amount of martensitic transformation is less compared to low loading rate. It appears that, martensitic transformation is exhausted during the later stages of deformation. As we can see from Fig. 6(a), at low loading rate, martensitic transformation is more uniformly distributed throughout the inclusion. At high loading rate martensitic transformation is accumulated close to the center of the inclusion.

3.2. Effect of transformation induced plasticity on crack propagation

Crack length is a Parameter that is helpful for comparing fracture toughness of different materials. As shown in Fig. 8(a), different RVE's have different crack length i.e., FM-DP RVE shows larger crack length, followed by TRIP and is least in FA-DP RVE. The cracks in all three RVEs move almost at the same speed till the crack tip reaches the in-clusion. But, inside the inclusion, the rate of crack growth varies, de-pending on the material properties of the inclusion. Crack moves rather quickly in martensite inclusion than in austenite inclusion. The crack propagation is considerably smoother in TRIP inclusion, as compared with austenite inclusion, because of the formation of martensite. As seen from the plot of crack length evolution (Fig. 8(a)), curves of FM-DP-RVE and FA-DP-RVE form the upper bound and the lower bound for that of TRIP-RVE.

It is clear from the results that, the crack propagates easily in martensite than in austenite inclusion. This fact is noted previously in many literatures [43,33,42]. In TRIP-RVE, because of the additional strain hardening, caused by newly formed martensite, crack propagation is hindered till the transformation is complete. However, once the transformation is complete, the rate of crack growth increases inside the inclusion, because of material property of newly formed martensite. This fits well to experiments and simulations reported by [37,26], that crack propagation is easier in martensite.

3.2.1. Orientation dependence of crack propagation

From the Fig. 8(b), it is clear that the crack length is higher in the

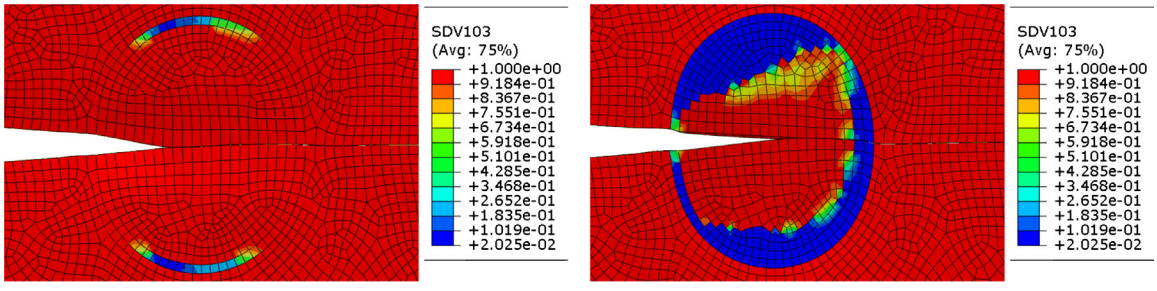

(a) Loading rate = 0.004 s^{-1}

(b) Loading rate = 0.0225 s^{-1}

Fig. 6. Martensitic volume fraction inside the TRIP-RVE inclusion, at two different loading rates. Orientation for retained austenite inclusion is (0, 0, 0). Blue cells in the inclusion shows the untransformed retained austenite. SDV represents the amount of martensitic transformation in the scale of 0 (untransformed) – 1 (completely transformed). (For interpretation of the references to color in this figure legend, the reader is referred to the web version of this article.)

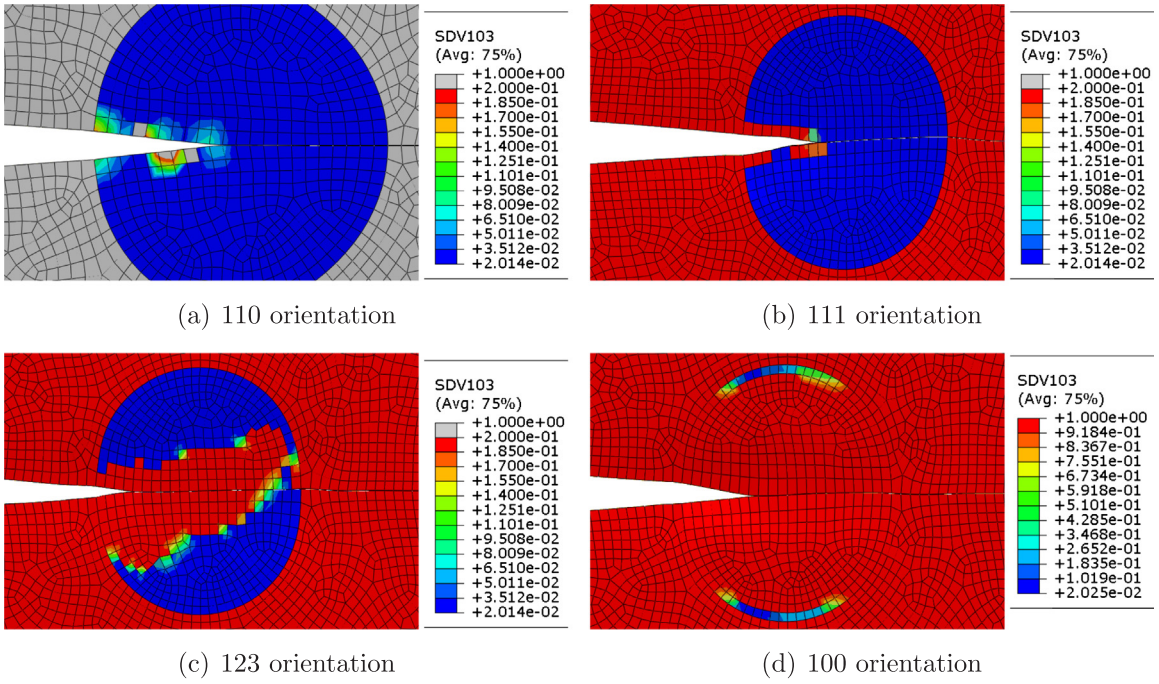

(a) 110 orientation (b) 111 orientation

(c) 123 orientation (d) 100 orientation

Fig. 7. Martensitic volume fraction inside the TRIP-RVE inclusion, for different retained austenite inclusion orientation at t = 100 (0.004 s^{-1} loading rate). Blue cells in the inclusion shows the untransformed retained austenite. SDV represents the amount of martensitic transformation in the scale of 0 (untransformed) – 1 (completely transformed).

[1 1 0] oriented inclusions, followed by [1 1 1], [1 2 3], [1 0 0]. This behaviour can be explained with the help of the amount of martensitic transformation and the stress state inside the inclusion. The crack propagation is easier in the [1 1 0], [1 1 1] oriented retained austenite inclusions, because of the initial higher stress levels (as shown in Fig. 4) and the amount of martensitic volume fraction. These two factors combined together make it easy for crack propagation. For [1 0 0], [1 2 3] oriented inclusions, the stress values inside the inclusion is low when compared with other two orientations, also the amount of martensitic transformation is high, hence, making it least favourable for crack propagation. This further supports the argument that transfor-mation of austenite to martensite hinders crack propagation.

The study on crack length is performed for both loading rates (0.0225 s^{-1} and 0.004 s^{-1}). But, results presented above are only for loading rate 0.004 s^{-1}, because there is not much difference in the overall behaviour or in the order of crack length (FM-DP-RVE still has highest crack length) at loading rate 0.0225^{-1}. At high loading rate, only the absolute values of crack lengths will increase linearly for all RVE's, including different RA orientations.

3.3. Crack path

In this section, results for relative activity of inclusion cracking and interface debonding is presented. In order to study the factors influencing crack path, uniaxial tensile tests were performed at two different loading rates (i.e. higher (0.0225 s^{-1}) and lower (0.004 s^{-1}) loading rate) and six different cohesive strength ratios. For convenience the interfacial strength (relative interfacial strength) is represented by

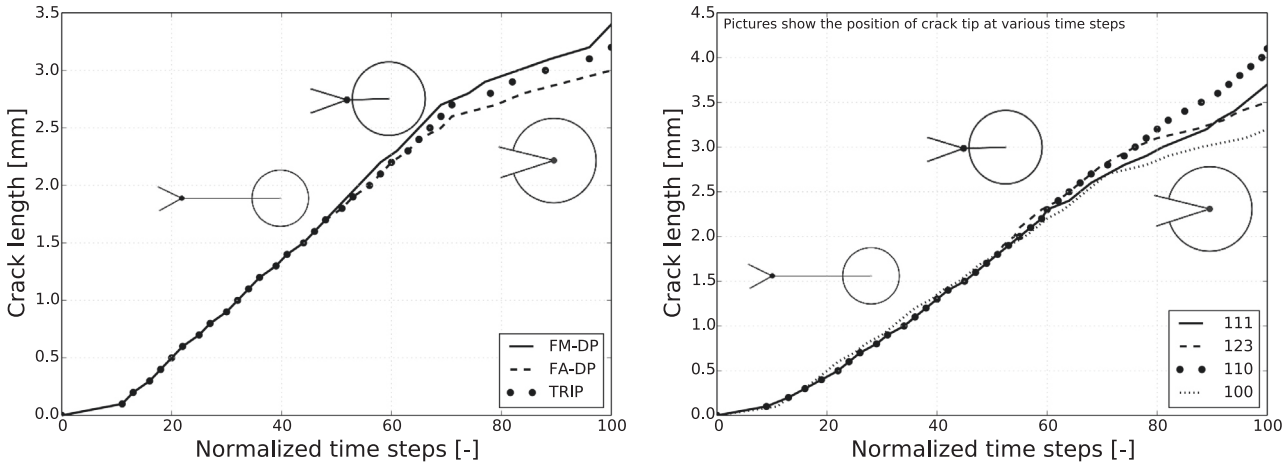

(a) Crack length for different RVE's (b) Effect of retained austenite inclusion orientation on crack length in TRIP RVE

Fig. 8. Crack length – normalized time steps for different RVE's (loading rate of 0.004 s^{-1}).

dimensionless ratio of interfacial cohesive strength to that of inclusion cohesive strength. G_{int}/G_{inc}, G_{inc} – inclusion cohesive strength, G_{int} – interface cohesive strength.

With the above mentioned loading rates and cohesive strength ratios, a total of 12 cases were studied, for each RVE's. As shown in Figs. 10, 12, 13, both loading rate and cohesive strength ratios influ-ence crack prorogation direction strongly.

The relative activity of inclusion cracking and interface debonding has been the topic of study for many years. Various numerical models have been used to predict this activity. The results presented below is similar to the behaviour reported by He and Hutchinson [8] in their analytical study on inclusion under static loading condition. The crack deflection or penetration behaviour, as shown in Fig. 10 can be explained as follows. A matrix crack in a homogeneous material should propagate along its self similar direction. However, introduction of an interface as a weaker strength direction results in energy distribution, leading the crack to deflect and propagate along the interface. If the interface strength is weaker, it is easier for satisfying the damage criterion and hence crack must propagate along the interface. But, when the interface strength is very high, the crack has to propagate inside the inclusion, because the interface cannot be fractured.

There exists a critical cohesive strength ratio for each loading rate, that decides whether crack penetrates into inclusion or deflects into the interface. Here, the deflection mechanism means, the crack propagates from the ferrite matrix towards the inclusion and chooses the matrix-inclusion interface as a new prorogation direction, as shown in Fig. 9(b). The penetration mechanism means, the crack propagates from the ferrite matrix towards the inclusion and runs into the inclusion taking a self similar direction, as shown in Fig. 9(a).

For FM-DP-RVE, it is clear from Fig. 10(b) that there is a critical cohesive strength ratio, which distinguishes between intergranular and transgranular mode of failure. The critical cohesive strength ratio at high loading rate is 0.7 and at low loading rate it is 0.8. For FM-DP-RVE, the interface debonding is dominating mechanism irrespective of the loading rate. This is because of the presence of martensite inclusion. With martensite inclusion, the difference in the hardness between martensite and ferrite is high, this causes strain incompatibility between ferrite matrix and martensite inclusion, this is a well known fact from experimental results Pardoen [34]. The difference in the strain levels between the ferrite matrix and martensite inclusion is clearly evident from Fig. 11, this induces rapid debonding along the interface. For FM-DP-RVE, when the loading rate increases from 0.004 s^{-1} to 0.0225 s^{-1}, the critical cohesive energy ratio drops from 0.85 to 0.75, it is clear from the results that the cohesive strength ratio depends on the loading rate.

For FA-DP-RVE, the critical cohesive strength ratio is 0.5 at both the loading rate as shown in Fig. 10(a). This clearly indicates that, with austenite inclusion, inclusion cracking is the favourable mechanism. This is because of strain compatibility at the interface between ferrite matrix and austenite inclusion. Even though, crack favours entering austenite inclusion, it is not easy for crack propagation inside the austenite inclusion, because of ductile nature of austenite. This is clearly evident from the value of crack length, as shown in Fig. 8(a).

For TRIP-RVE, the critical cohesive strength ratio at high loading rate is 0.5 and at low loading rate it is 0.8. From Fig. 12(a), we can see that, at high loading rate crack prefers going into the inclusion and at low loading rate, interface debonding dominates. This can be explained based on the stress state inside the inclusion, strain incompatibility at the interface and martensitic transformation inside the inclusion. The behaviour of inclusion with TRIP is similar to that of the martensite at lower loading rate, but at higher loading rate, the critical cohesive strength ratio is lesser than martensite inclusion. At higher loading rate, the stress state inside the inclusion is higher compared to low loading rate, also, the time for energy distribution into weaker paths is very less, this makes the crack to continue in the same direction as before. Also, at high loading rate, the martensitic transformation rate in the inclusion is very fast (as shown in Fig. 5(b)) and the transformation appears to be exhausted very quickly, leaving some amount of retained austenite near to interface untransformed (as we can see from Fig. 6(b)). With much softer retained austenite at the interface, there is not much strain incompatibility at the interface, hence creating a favourable condition for crack to move into inclusion. But, after certain strength ratio (critical interface strength), the interface will be very weak and the condition for damage initiation is easily satisfied as the cohesive strength of in-terface is very low, promoting interface debonding. On contrary, at low loading rate, the transformation of austenite to martensite is more uniform and complete, this means that, even the retained austenite close to interface also transforms Fig. 6(a). This creates favourable condition for interface debonding, as there is strain incompatibility, similar to martensite inclusion.

From the above results, it is clear that the material property of the inclusion plays an important role in deciding the crack path, along with cohesive strength ratio, applied loading rate, phase transformation of retained austenite to martensite. As we can see from Fig. 7, orientation of the retained austenite inclusion is an important factor that can affect phase transformation, hence the stress and strain state inside the inclusion. Therefore, orientation of the retained austenite is also considered for studying the crack path. In the section below, results for, influence of retained austenite inclusion orientations are presented.

3.3.1. *Crack path and orientation dependence*

Simulations for determining the effect of retained austenite orientation, on the relative activity of inclusion cracking and interface debonding are performed using same boundary condition and RVE's as discussed in previous section, except that the orientation of the retained austenite is varied for different cases.

As seen from Figs. 12 and 13, orientation dependence of the crack path is clearly evident. For [1 1 1], [1 1 0] orientations, the crack path behaviour is similar to that of FA-DP-RVE i.e., inclusion cracking is the favourable mechanism. This is because of lack of martensitic transfor-mation in these orientations, leaving behind large amount of austenite Fig. 7(a) and (b). As mention in previous section, with austenite in-clusion, there is no strain incompatibility at the interface. Apart from this, because of the orientation of the inclusions, stress inside the

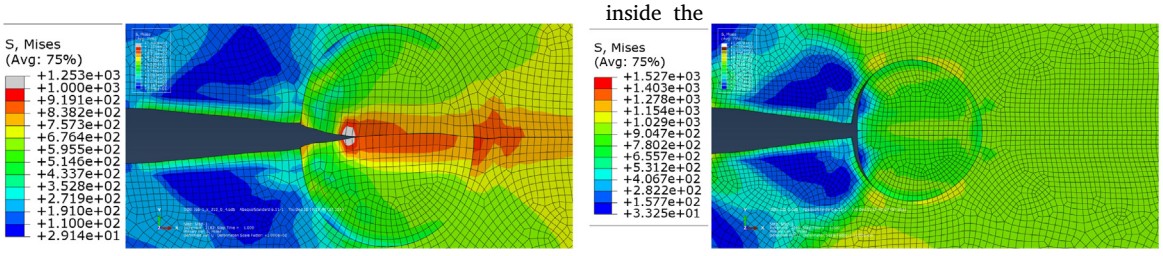

(a) Inclusion cracking. (b) Interface debonding of inclusion.

Fig. 9. Schematic representation of inclusion cracking and interface debonding in TRIP RVE with retained austenite inclusion orientation (0, 0, 0), at loading rate 0.004 s^{-1}.

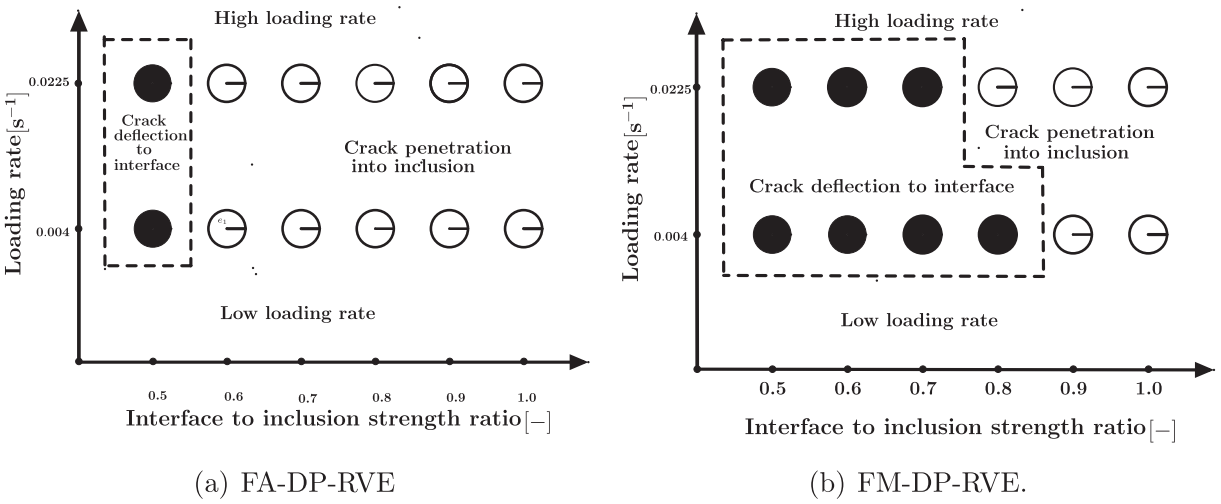

Fig. 10. Influence of loading rate and cohesive strength ratio on crack path (Shaded circle represents the inclusion cracking and hollow circle represents the interface debonding).

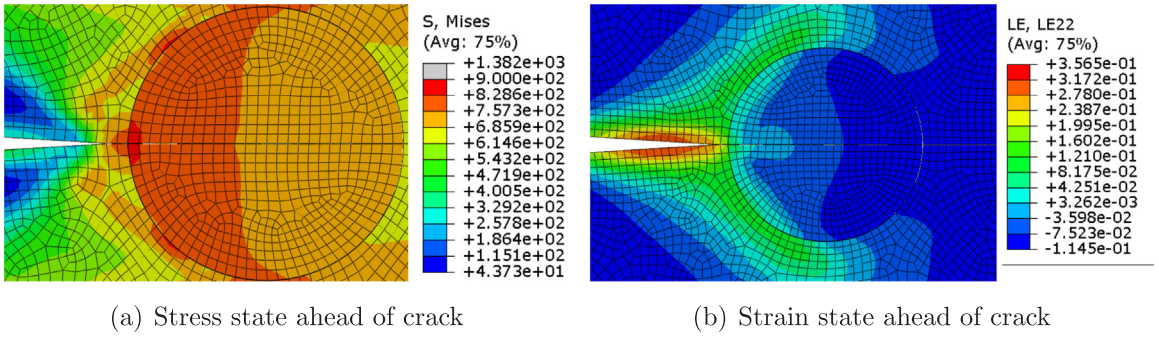

Fig. 11. Stress and strain state in front of crack, before interface debonding for FM-DP-RVE at t = 60.

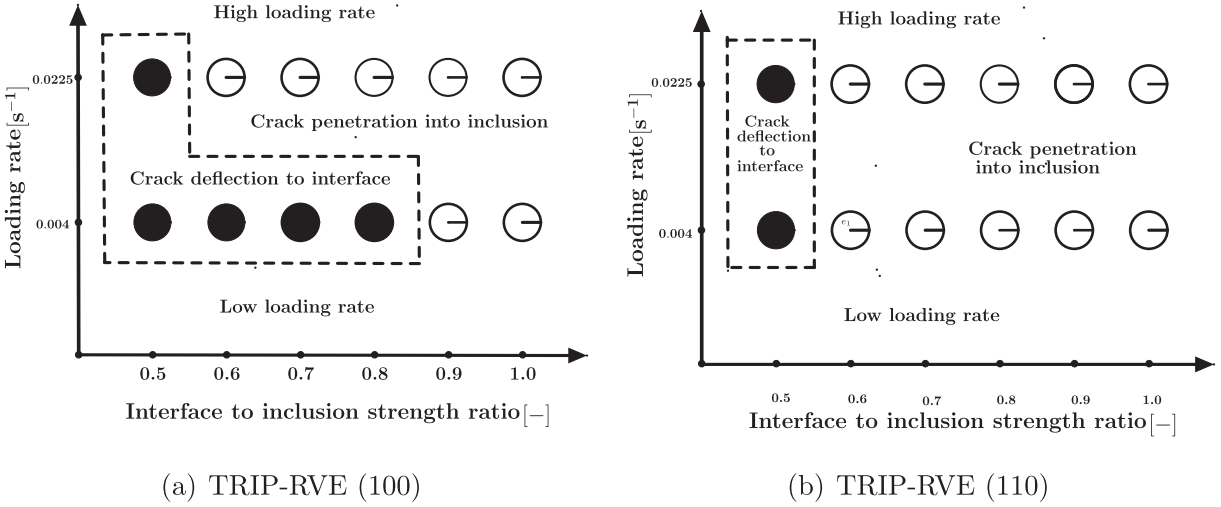

Fig. 12. Influence of loading rate and cohesive strength ratio on crack path (Shaded circle represents the inclusion cracking and hollow circle represents the interface debonding).

inclusion is also high, which is favourable for crack propagation inside the inclusion. The crack chooses interface only when the value of interface strength is very low (i.e., at low ratio), this trend is common for both the loading rates considered in the study. The only difference between these two orientations and FA-DP-RVE is the crack length, as we can see from Fig. 8, the crack propagation is easier in TRIP RVE's with [1 1 1], [1 1 0] orientations than in FA-DP-RVE.

For TRIP RVE with retained austenite inclusion orientation [1 2 3] Fig. 13(b), the critical cohesive strength ratio at high loading rate is 0.6 and at low loading rate it is 0.7. The behaviour is similar to that of [1 0 0] orientation. The crack favours inclusion cracking rather than interface debonding at high loading rates, but at low loading rate both inclusion cracking and interface debonding are equally favourable. The main difference between [1 2 3] and [1 0 0] orientations is the crack length, for RA inclusion with [1 2 3] orientation, crack propagation is easier Fig. 8(b).

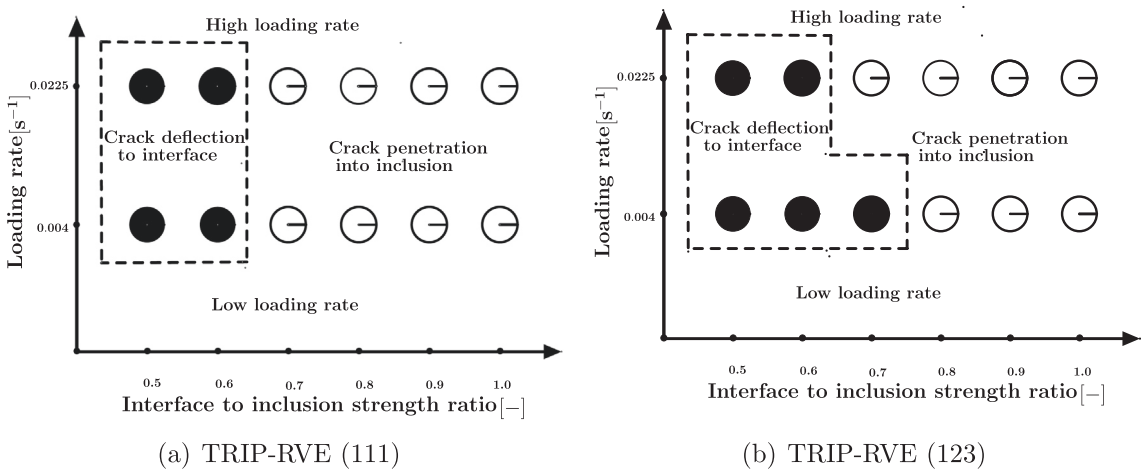

Fig. 13. Influence of loading rate and cohesive strength ratio on crack path (Shaded circle represents the inclusion cracking and hollow circle represents the interface debonding).

4. Conclusion

In the present work, an advanced crystal plasticity and phase transformation model has been employed to study crack propagation, in several specifically designed RVEs. The constitutive model, used here considered many important physical mechanisms such as relation between the strain induced martensite nucleation and plastic deformation of meta-stable austenite, and also considers stress assisted growth and strain induced nucleation at the same time. Cracks inside aforementioned RVEs were simulated by a phenomenological cohesive zone model. Different RVE's are created with ferrite matrix and retained austenite inclusion.

From the numerical simulation, the following conclusions are drawn:

- Transformation induced plasticity improves strength and ductility of multiphase steels efficiently. The martensite phase transformation is found to have significant effect on the crack propagation, the transformation induced plasticity hinders crack propagation.
- The crack penetration or deflection around the retained austenite or martensite inclusion, depends on various factors like cohesive strength, loading rate and orientation of retained austenite inclusion. Interface debonding is the favourable mechanism for ferrite matrix with martensite inclusion. For ferrite matrix with austenite inclusion without transformation, inclusion cracking is the favourable mechanism.
- Orientation of retained austenite inclusion affects the amount of martensitic transformation and stress state inside the inclusion, i.e., among the investigated orientations, [1 0 0] and [1 1 0] are the most favourable and most unfavourable orientations for martensitic transformation.

Acknowledgements

The authors would like to thank Prof. Dr. Alexander Hartmaier for his valuable suggestions and fruitful discussions.

References

[1] Abaqus, Dassault Systemes Abaqus 6.11 Documentation, 2011.
[2] G. Avramovic-Cingara, Y. Ososkov, M. Jain, D. Wilkinson, Effect of martensite distribution on damage behaviour in {DP600} dual phase steels, Mater. Sci. Eng.: A 516 (2009) 7–16.
[3] K. Bhadeshia, Trip-assisted steels? ISIJ Int. 42 (2002) 1059.
[4] M. Erdogan, The effect of new ferrite content on the tensile fracture behaviour of dual phase steels, J. Mater. Sci. 37 (2002) 3623–3630.
[5] F.L.Q. Furnémont, T.V. Rompaey, F. Delannay, P. Jacques, T. Pardoen, Multiscale mechanics of trip-assisted multiphase steels: II. Micromechanical modelling, Acta Mater. 55 (11) (2007) 3695–3705.
[6] T. de Geus, R. Peerlings, M. Geers, Competing damage mechanisms in a two-phase microstructure: how microstructure and loading conditions determine the onset of fracture, Int. J. Solids Struct. (2016).
[7] S. Gupta, A. Ma, A. Hartmaier, Investigating the influence of crystal orientation on bending size effect of single crystal beams, Comput. Mater. Sci. 101 (2015) 201–210.
[8] M.Y. He, J.W. Hutchinson, Crack deflection at an interface between dissimilar elastic materials, Int. J. Solids Struct. 25 (9) (1989) 1053–1067.
[9] X.J. He, N. Terao, A. Berghezan, Influence of martensite morphology and its dispersion on mechanical properties and fracture mechanisms of Fe-Mn-C dual phase steels, Met. Sci. 18 (1984) 367–373.
[10] S.S. Hecker, M.G. Stout, K.P. Staudhammer, J.L. Smith, Effects of strain state and strain rate on deformation-induced transformation in 304 stainless steel: Part I. Magnetic measurements and mechanical behavior, Metall. Trans. A 13 (1982) 619–626.
[11] P. Jacques, Transformation-induced plasticity for high strength formable steels, Curr. Opin. Solid State Mater. Sci. 8 (2004) 259–265.
[12] P. Jacques, Transformation-induced plasticity for high strength formable steels, Curr. Opin. Solid State Mater. Sci. 8 (3–4) (2004) 259–265.
[13] P. Jacques, Q. Furnémont, A. Mertens, F. Delannay, On the sources of work hardening in multiphase steels assisted by transformation-induced plasticity, Philos. Mag. A 81 (2001) 1789–1812.
[14] P. Jacques, Q. Furnémont, T. Pardoen, F. Delannay, On the role of martensitic transformation on damage and cracking resistance in trip-assisted multiphase steels, Acta Mater. 49 (2001) 139–152.
[15] J. Kadkhodapour, A. Butz, S.Z. Rad, Mechanisms of void formation during tensile testing in a commercial, dual-phase steel, Acta Mater. 59 (2011) 2575–2588.
[16] J. Kadkhodapour, A. Butz, S. Ziaei-Rad, S. Schmauder, A micro mechanical study on failure initiation of dual phase steels under tension using single crystal plasticity model, Int. J. Plast. 27 (2011) 1103–1125.
[17] J. Kang, Y. Ososkov, J.D. Embury, D.S. Wilkinson, Digital image correlation studies for microscopic strain distribution and damage in dual phase steels, Scr. Mater. 56 (2007) 999–1002.
[18] J. Koo, Design of Duplex Low Carbon Steels for Improved Strength: Weight Applications, Lawrence Berkeley National Laboratory, 2010.
[19] G. Lacroix, T. Pardoen, P. Jacques, The fracture toughness of trip-assisted multiphase steels, Acta Mater. 56 (15) (2008) 3900–3913.
[20] F. Lani, Q. Furnémont, T.V. Rompaey, F. Delannay, P. Jacques, T. Pardoen, Multiscale mechanics of trip-assisted multiphase steels: I. Micromechanical modelling, Acta Mater. 55 (11) (2007) 3681–3693.
[21] F. Lani, Q. Furnémont, T.V. Rompaey, F. Delannay, P. Jacques, T. Pardoen, Multiscale mechanics of trip-assisted multiphase steels: II. Micromechanical modelling, Acta Mater. 55 (11) (2007) 3695–3705.
[22] A. Lebedev, V. Kosarchuk, Influence of phase transformations on the mechanical properties of austenitic stainless steels, Int. J. Plast. 16 (2000) 749.
[23] A. Ma, A. Hartmaier, A study of deformation and phase transformation coupling for trip-assisted steels, Int. J. Plast. 64 (2015) 40–55.
[24] E. Maire, O. Bouaziz, M. Di Michiel, C. Verdu, Initiation and growth of damage in a dual-phase steel observed by x-ray microtomography, Acta Mater. 56 (2008) 4954–4964.
[25] H.R. Mayer, S.E. Stanzl-Tschegg, Y. Sawaki, M. Hühner, E. Hornbogen, Influence of transformation-induced crack closure on slow fatigue crack growth under variable amplitude loading, Fatigue Fract. Eng. Mater. Struct. 18 (1995) 935–948.
[26] Z. Mei, J.W. Morris, Influence of deformation-induced martensite on fatigue crack propagation in 304-type steels, Int. J. Mater. Res. 21 (1990) 3137–3152.
[27] O. Muransky, P. Sittner, In situ neutron diffraction investigation of the collaborative deformation–transformation mechanism in trip-assisted steels at room and elevated

temperatures, Acta Mater. 56 (14) (2008) 3367–3379.
[28] L.E. Murr, K.P. Staudhammer, S.S. Hecker, Effects of strain state and strain rate on deformation-induced transformation in 304 stainless steel: Part II. Microstructural study, Metall. Trans. A 13 (1982) 627–635.
[29] A.H. Nakagawa, G. Thomas, Microstructure-mechanical property relationships of dual-phase steel wire, Metall. Trans. A 16 (1985) 831–840.
[30] G. Olson, M. Azrin, Transformation behavior of trip steels, Metall. Trans. A 9 (1978) 713–721.
[31] G. Olson, M. Cohen, Kinetics of strain-induced martensitic nucleation, Metall. Trans. A 6 (1975) 791–795.
[32] S. Papaefthymiou, U. Prahl, W. Bleck, S. van der Zwaag, J. Sietsma, Experimental observations on the correlation between microstructure and fracture of multiphase steels: dedicated to professor Eckard Macherauch on the occasion of the 80th anniversary of his birth, Z. Metall. 97 (2006) 1723–1731.
[33] S. Papaefthymiou, U. Prahl, W. Bleck, S.V.D. Zwaag, J. Sietsma, Experimental observations on the correlation between microstructure and fracture of multiphase steels, Int. J. Mater. Res. 97 (2006) 1723–1731.
[34] T. Pardoen, Numerical simulation of low stress triaxiality ductile fracture, Comput. Struct. 84 (2006) 1641–1650.
[35] M. Rashid, Dual phase steels, Annu. Rev. Mater. Sci. 11 (1981) 245–266.
[36] G. Satyapriya, T. Raphael, K. Pawel, M. Sebastian, Experimental and numerical investigations of the TRIP effect in 1.4301 austenitic stainless steel under static loading, Steel Res. Int. 85 (2014) 793–802.
[37] S.J. Suiker, S. Turteltaub, Numerical modelling of transformation-induced damage and plasticity in metals, Modell. Simul. Mater. Sci. Eng. 15 (2007) S147.
[38] C.C. Tasan, M. Diehl, D. Yan, M. Bechtold, F. Roters, L. Schemmann, C. Zheng, N. Peranio, D. Ponge, M. Koyama, et al., An overview of dual-phase steels: advances in microstructure-oriented processing and micromechanically guided design, Annu. Rev. Mater. Res. 45 (2015) 391–431.
[39] D.D. Tjahjanto, S. Turteltaub, A.S.J. Suiker, Crystallographically based model for transformation-induced plasticity in multiphase carbon steels, Continuum Mech. Thermodyn. 19 (2008) 399–422.
[40] D.D. Tjahjanto, S. Turteltaub, A.S.J. Suiker, S. van der Zwaag, Modelling of the effects of grain orientation on transformation-induced plasticity in multiphase carbon steels, Modell. Simul. Mater. Sci. Eng. 14 (2006) 617.
[41] Y. Tomota, H. Tokuda, Y. Adachi, Tensile behavior of trip-aided multi-phase steels studied by in situ neutron diffraction, Acta Mater. 52 (20) (2004) 5737–5745.
[42] V. Uthaisangsuk, U. Prahl, W. Bleck, Micromechanical modelling of damage behaviour of multiphase steels, Comput. Mater. Sci. 43 (2008) 27–35 Proceedings of the 16th International Workshop on Computational Mechanics of MaterialsIWCMM-16..
[43] V. Uthaisangsuk, U. Prahl, W. Bleck, Modelling of damage and failure in multiphase high strength {DP} and {TRIP} steels, Eng. Fract. Mech. 78 (2011) 469–486 Meso-Mechanical Modelling of Fatigue and Fracture..